



THE UNIVERSITY *of* EDINBURGH

Edinburgh Research Explorer

## **Poly-epsilon-lysine hydrogels with dynamic crosslinking facilitates cell proliferation**

### **Citation for published version:**

Lopez Mora, N, Simmonte Owens, M, Schmidt, S, Fonseca Da Silva, A & Bradley, M 2020, 'Poly-epsilon-lysine hydrogels with dynamic crosslinking facilitates cell proliferation', *Materials*, vol. 13, no. 17.  
<https://doi.org/10.3390/ma13173851>

### **Digital Object Identifier (DOI):**

[10.3390/ma13173851](https://doi.org/10.3390/ma13173851)

### **Link:**

[Link to publication record in Edinburgh Research Explorer](#)

### **Document Version:**

Peer reviewed version

### **Published In:**

Materials

### **General rights**

Copyright for the publications made accessible via the Edinburgh Research Explorer is retained by the author(s) and / or other copyright owners and it is a condition of accessing these publications that users recognise and abide by the legal requirements associated with these rights.

### **Take down policy**

The University of Edinburgh has made every reasonable effort to ensure that Edinburgh Research Explorer content complies with UK legislation. If you believe that the public display of this file breaches copyright please contact [openaccess@ed.ac.uk](mailto:openaccess@ed.ac.uk) providing details, and we will remove access to the work immediately and investigate your claim.



1 Article

# 2 Poly-epsilon-lysine hydrogels with dynamic 3 crosslinking facilitates cell proliferation

4 Nestor Lopez Mora,<sup>1,\*</sup> Matthew Owens,<sup>1</sup> Sara Schmidt,<sup>1</sup> Andreia F. Silva,<sup>2</sup> and Mark Bradley.<sup>1,\*</sup>

5 <sup>1</sup> EaStCHEM School of Chemistry, The University of Edinburgh, Edinburgh EH9 3FJ, UK.

6 <sup>2</sup> School of Physics and Astronomy, The University of Edinburgh, Edinburgh EH9 3FD, UK.

7 \* Correspondence: [nesfab@gmail.com](mailto:nesfab@gmail.com) (N.L.M.); [mark.bradley@ed.ac.uk](mailto:mark.bradley@ed.ac.uk) (M.B.); Tel.: +44-0131-650-4820 (M.B.).

8 Received: date; Accepted: date; Published: date

9 **Abstract:** The extracellular matrix (ECM) is a three-dimensional network within which fundamental  
10 cell processes such as cell attachment, proliferation, and differentiation occur driven by its inherent  
11 biological and structural cues. Hydrogels have been used as biomaterials as they possess many of  
12 the ECM characteristics that control cellular processes. However, the permanent crosslinking often  
13 found in hydrogels fails to recapitulate the dynamic nature of the natural ECM. This not only  
14 hinders natural cellular migration but must also limit cellular expansion and growth. Moreover,  
15 there is an increased interest in the use of new biopolymers to create biomimetic materials that can  
16 be used for biomedical applications. Here we report on the natural polymer poly- $\epsilon$ -lysine in forming  
17 dynamic hydrogels *via* reversible imine bond formation, with cell attachment promoted by RGD  
18 incorporation. Together, the mechanical properties, and cell behavior on the dynamic hydrogels  
19 with low poly- $\epsilon$ -lysine quantities indicated good cell viability, and high metabolic activity.

20 **Keywords:** Dynamic hydrogels, poly- $\epsilon$ -lysine, RGD peptide, imine crosslinking, 4-arm PEG.

21

## 22 1. Introduction

23 Hydrogels are highly hydrated three-dimensional (3D) polymer networks that have been used  
24 for a broad range of biomedical applications that range from tissue engineering [1,2], and surgical  
25 glues [3,4], to contact lenses [5,6], materials for drug delivery [7], and biosensors [8]. In large part this  
26 is due to their tunable mechanical properties and their biocompatibility [9]. The high water content  
27 of these 3D macromolecular networks and the ability to decorate them with ligands creates an ideal  
28 environment for diffusion and transport of nutrients, while offering optimal characteristics for  
29 generating a 3D cell culture matrix. However, the high degree of crosslinking in hydrogels, necessary  
30 to provide stability and structural support to cells, creates a static polymer network that hinders cell  
31 migration, a critical feature of the dynamic environment of the natural extracellular matrix (ECM)  
32 [10]. Cell migration has been achieved by the introduction of hydrogel degradability with, for  
33 example, the incorporation of hydrolytically degradable polylactide segments [11,12], or substrates  
34 of degradative enzymes such as metalloproteases [13,14], but in these cases the material is  
35 permanently broken down leading to material collapse over time. Recently, using dynamic covalent  
36 chemistry [15], hydrogel networks with exchangeable, reversible, or adaptable linkages have been  
37 formed through Diels-Alder [16], hydrazine [17], Schiff's base (imine) [18], oxime [19], and disulfide  
38 [20], bond formation. The dynamic bond breakage and reformation generates a rearranging  
39 molecular network that allows cells to move and spread throughout the 3D polymer network [21],  
40 opening a new set of potential properties such as self-healing [22,23], shape memory [24], and stimuli-  
41 responsiveness [25-27], enhancing their potential use in biomedical applications.

42 ECM mimics have been successfully generated using numerous synthetic polymers, creating  
43 hydrogels with unique structural and mechanical properties for use as structural cellular supports  
44 [28]. In the majority of cases the desired characteristics include controllable matrix stiffnesses and cell

45 biocompatibility, resulting in optimal cell adhesion and survival [29]. Despite the advances in  
46 synthetic biomaterials, there is considerable interest in using naturally occurring polymers to create  
47 biomimetic materials for biomedical applications. Biopolymers previously explored include chitosan  
48 [30,31], alginate [32,33], gelatine [34], and hyaluronic acid [35], which have been functionalized and  
49 used as biopolymer precursors to form dynamic hydrogels. This creates a responsive structure akin  
50 to the natural ECM and allows for *in situ* cell encapsulation. The hydrogel/cell association can be  
51 further enhanced with the incorporation of peptides [36], proteins such as growth factors [37],  
52 polysaccharides and proteoglycans [38], or synthetic analogues, thus allowing biological properties  
53 such as cell attachment, proliferation, and differentiation, to be introduced and modulated. The  
54 peptide motif arginine-glycine-aspartic acid (RGD) is a peptide adhesion sequence found in many  
55 ECM proteins such as fibronectin, fibrinogen, vitronectin, and laminin as a specific integrin ligand  
56 [39-41]. Many aspects of the RGD motif such as structure [42,43], spacing [44], and density  
57 distribution [45-47], have been studied, with synergism between the biomechanical properties of the  
58 polymer matrix and the RGD motif modulating the cellular adhesive response. Additionally, plasma  
59 protein binding onto RGD-functionalized biomaterials further passivates the surface and promotes  
60 cellular binding.

61 Poly- $\epsilon$ -lysine is a natural homo-poly-amino acid used as an emulsifier and preservative in the  
62 food industry (with FDA certification [48]) that is nontoxic towards humans [49,50], and has been  
63 demonstrated to be biocompatible [51]. Herein, the naturally occurring poly- $\epsilon$ -lysine, without further  
64 functionalization, was exploited in the design of arrays of dynamic hydrogels that were crosslinked  
65 *via* reversible Schiff-base bond formation with a 4-armed PEG-aldehydes. There are a limited number  
66 of studies with hydrogels including poly- $\epsilon$ -lysine [52], or modified versions of poly- $\epsilon$ -lysine [53], to  
67 form conventional chemically crosslinked hydrogels, for example *via* amide bond crosslinking. To  
68 the best of our knowledge, however, no designed dynamic poly- $\epsilon$ -lysine hydrogels have been  
69 proposed as ECM mimics [54]. This is perhaps due to the relative weakness of the reversible  
70 crosslinking that produces softer hydrogels in comparison to stiff static hydrogels produced with  
71 conventional chemical crosslinking. Contrary to our initial hypothesis that the high amount of amine  
72 groups distributed along the poly- $\epsilon$ -lysine backbone would be detrimental to cell viability, high cell  
73 viability was observed on the poly- $\epsilon$ -lysine dynamic hydrogels (HG-P $\epsilon$ K) formulated at low ratios of  
74 poly- $\epsilon$ -lysine. Additionally, the linear poly- $\epsilon$ -lysine backbone led to a suitable network with the  
75 required biomaterial stiffness to afford cell structural support and proliferation. To aid cellular  
76 adhesion and binding specificity, the linear peptide H-Ahx-GRGDSK-NH<sub>2</sub> (referred to here as RGD)  
77 with primary amines at both the amino and carboxyl termini (*via* the lysine residue) was incorporated  
78 during hydrogel formulation. An RGD linear structure was selected over the cyclic analogue based  
79 on a previous report that showed improved long-term cellular adhesion [55]. A range of RGD  
80 concentrations was explored to determine cellular adhesion and survival on HG-P $\epsilon$ K. The HG-P $\epsilon$ K  
81 was compared to a similar dynamic hydrogel made of the non-fouling polymer poly(ethylene glycol)  
82 (HG-PEG) to isolate the RGD contribution to cell binding properties, with higher performance found  
83 for HG-P $\epsilon$ K compared to HG-PEG.

## 84 2. Materials and Methods

85 *Materials.* 4-arm PEG-OH (10,000 Da), and H<sub>2</sub>N-PEG-NH<sub>2</sub> (2,000 Da) were purchased from  
86 JenKem Technologies. Poly- $\epsilon$ -lysine (3,500 – 4,000 Da) was purchased from Carbosynth. All amino  
87 acids, aminomethyl polystyrene resin, and the Fmoc-Rink amide linker were purchased from GL  
88 Biochem (Shanghai) Ltd. or NovaBiochem. All other chemicals were purchased from Sigma Aldrich  
89 or Acros and used without further purification, unless otherwise indicated. Dulbecco's Modified  
90 Eagle Medium (DMEM), LIVE/DEAD Cell Imaging Kit (488/570 nm) and AlamarBlue® cell viability  
91 reagent were purchased from Thermo Fisher. Phosphate-buffered saline (PBS) was purchased from  
92 Sigma Aldrich. DMEM was prepared with 10% fetal bovine serum (FBS), 100 U/mL penicillin, 100  
93  $\mu$ g/mL streptomycin and 2 mM glutamine (referred to as complete DMEM). 4-arm PEG-aldehydes  
94 with > 90% end group functionalization was synthesized following a method reported elsewhere (see  
95 Figure S1 and S2 in Supplementary Materials) [56]. HeLa cells were purchased from American Type

96 Culture Collection and cultured in 25 cm<sup>2</sup> flasks (Corning) using complete DMEM, with passage  
97 every 2-3 days using Trypsin-EDTA (Sigma).

98 *RGD solid-phase synthesis.* Linear H-Ahx-GRGDSK-NH<sub>2</sub> with a 6-aminohexanoic acid (Ahx)  
99 spacer at the N-terminus was synthesized on amino methyl polystyrene resin, functionalized with an  
100 Fmoc-Rink linker, using Fmoc/tBu solid-phase synthesis. The peptide was cleaved for 3 hours in a  
101 cleavage cocktail of 95% trifluoroacetic acid (TFA), 2.5% triisopropylsilane and 2.5% water with  
102 constant mixing at room temperature. The peptide was precipitated from the filtrate using cold  
103 diethyl ether, collected by centrifugation, and dried under vacuum. The RGD peptide was dissolved  
104 in 0.1% formic acid in water and purified by reversed-phase flash chromatography (Biotage Isolera)  
105 with a SNAP Ultra C18 column (Biotage). The solvents consisted of a mixture of 95% water/5%  
106 acetonitrile (0.1% formic acid; solvent A) and 100% acetonitrile (solvent B). A gradient of solvent B  
107 from 0 to 20% in 20 min, 20 to 95% in 5 minutes and 95% for 1 minute was used for peptide  
108 purification. The appropriate fractions were detected at  $\lambda = 214$  nm, combined, concentrated, and  
109 lyophilized. The peptide was characterized by analytical C18 reversed-phase HPLC (Agilent 1100  
110 ChemStation, USA) with an RGD peptide purity of > 95%, and HRMS (RGD m/z calculated 730.4086,  
111 m/z found 730.4127).

112 *Hydrogel formation.* Hydrogels were prepared by dynamic covalent crosslinking *via* Schiff's base  
113 formation. Stock polymer solutions were prepared by dissolving the 4-arm PEG-aldehydes, poly- $\epsilon$ -  
114 lysine or H<sub>2</sub>N-PEG-NH<sub>2</sub> to complete dissolution in PBS (pH 7.4) at room temperature. The hydrogel  
115 poly- $\epsilon$ -lysine (HG-P $\epsilon$ K) was prepared in 500  $\mu$ L batches varying the molar ratios of the 4-arm PEG-  
116 aldehydes and the lysine unit (in the poly- $\epsilon$ -lysine) (1:2 and 1:10) with a final polymer precursor  
117 weight of 10% w/v.

118 Thus, the HG-P $\epsilon$ K with a molar ratio of 1:2 was prepared by mixing stock solutions of 4-arm  
119 PEG-aldehydes (250  $\mu$ L, 20% w/v) with poly- $\epsilon$ -lysine (100  $\mu$ L, 5% w/v) and 150  $\mu$ L PBS. The HG-P $\epsilon$ K  
120 (molar ratio 1:10) was prepared by mixing stock solutions of the 4-arm PEG-aldehydes (250  $\mu$ L, 20%  
121 w/v) with poly- $\epsilon$ -lysine (130  $\mu$ L, 20% w/v) and 120  $\mu$ L PBS.

122 In a similar manner a non-fouling hydrogel was prepared by mixing 4-arm PEG-aldehydes (250  
123  $\mu$ L 20% w/v) with H<sub>2</sub>N-PEG-NH<sub>2</sub> (200  $\mu$ L, 20% w/v) and 50  $\mu$ L PBS. Following the same procedures,  
124 hydrogel constructs incorporating RGD were prepared at final concentrations of 0, 0.2, 2, 4, 6 and 20  
125 mM RGD with the addition of the stock RGD solution (100 mM in PBS) (see Table S1-S3 in  
126 Supplementary Materials). The pH of the final hydrogel solutions was measured immediately after  
127 mixing the precursor stock solutions with pH paper and before gelation. Gelation occurred within 2  
128 to 6 hours at room temperature.

129 *Rheological characterization.* Small amplitude oscillatory shear (SAOS) measurements were  
130 performed in duplicate using a strain-controlled ARES-G2 Rheometer (TA Instruments). A  
131 sandblasted plate-plate geometry (40 mm, stainless steel) with a gap of 300  $\mu$ m was used. Hydrogel  
132 samples of 500  $\mu$ L were measured. Time sweeps were performed at an angular frequency of 1 Hz and  
133 constant strain of 1% at 37 °C. Amplitude sweep experiments were performed for strains ( $\gamma$ ) between  
134 0.01 and 100% at constant frequency ( $\omega = 10$  rad/s), and it was found that for a strain of 1% both  
135 moduli were in the linear viscoelastic region (LVE). Frequency sweeps were performed with a  
136 constant strain of 1% for angular frequencies between 0.1 and 100 rad/s at 37 °C.

137 *Cryo-Scanning Electron Microscopy (cryo-SEM).* The internal structure of the hydrogel constructs  
138 was imaged in a Gemini 2 FIB-cryo-SEM (Zeiss). The hydrogel construct was placed in the sample  
139 holder and frozen with liquid nitrogen. The hydrogel was then freeze fractured with a scraper,  
140 sputtered with platinum, and imaged at 3.0 kV.

141 *Cell culture conditions.* A 96-well plate was passivated with a stock solution of poly-L-lysine  
142 (0.01% w/v), incubated for 10 minutes, drained, and dried overnight at room temperature. Hydrogel  
143 arrays of HG-P $\epsilon$ K and HG-PEG with RGD concentrations of 0, 0.2, 2, 4, 6 and 20 mM were made by  
144 transferring 50  $\mu$ L of each hydrogel construct into the previously functionalized 96-well plate or 10  
145  $\mu$ L on a Ibidi  $\mu$ -Slide Angiogenesis well plate (without surface passivation). After hydrogel  
146 formation, the 96-well plate or Ibidi  $\mu$ -Slide Angiogenesis well plate holding the hydrogel array was  
147 sterilized by UV light for 60 minutes, before rinsing the chambers with complete DMEM. HeLa cells

148 were seeded at a density of  $2 \times 10^4$  cells per well in a 96-well plate or a density of  $2.7 \times 10^3$  HeLa cells  
149 per well in the Ibidi  $\mu$ -Slide Angiogenesis well plate, and incubated at 37 °C, 5% CO<sub>2</sub>. Cell culture  
150 was maintained with complete DMEM exchanges every 48 hours.

151 *Live/Dead cell viability* analysis was performed using calcein AM for a live stain ( $\lambda_{\text{ex}}/\lambda_{\text{em}} = 488/515$   
152 nm) and propidium iodide as a dead stain ( $\lambda_{\text{ex}}/\lambda_{\text{em}} = 570/602$  nm) after 48 hours of *in vitro* cell culture  
153 in HG-PεK or HG-PEG with and without RGD. Fluorescence imaging was performed on a Zeiss  
154 AxioVert 200m fluorescence microscope for the 96-well plate hydrogel and laser scanning confocal  
155 microscopy on a Leica TCS SP8 confocal (CALM facilities, Queen's Medical Research Institute,  
156 Edinburgh, UK) for the Ibidi  $\mu$ -Slide Angiogenesis well plate and analyzed using the software  
157 ImageJ.

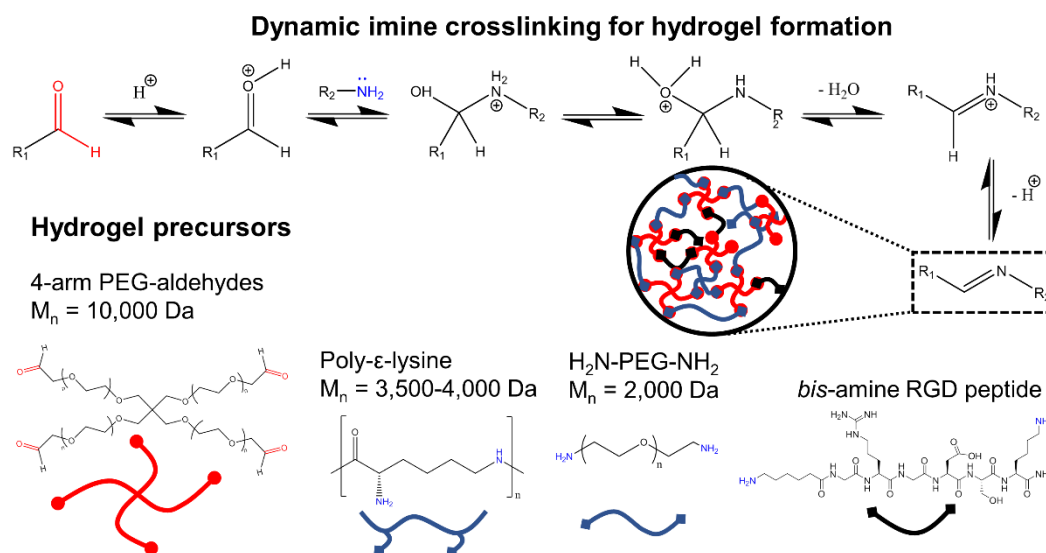
158 *AlamarBlue proliferation assays* were performed in 96-well plates holding the hydrogel construct  
159 array with measurement of AlamarBlue fluorescence after HeLa cell culture. HeLa cells were seeded  
160 in HG-PεK and HG-PEG with and without RGD at a cell density of  $2.0 \times 10^4$  cells per well and  
161 incubated with complete DMEM for 48 hours at 37 °C and 5% CO<sub>2</sub>. Subsequently, DMEM was  
162 removed and AlamarBlue (10% v/v, 200  $\mu$ L) in medium was added. An immediate baseline reading  
163 of fluorescence was taken at 590 nm using a BioTek HT Synergy multimode reader with Gen 5.2.06.10  
164 software. The cell seeded gels were then incubated for 5 hours and remeasured for fluorescence, with  
165 subtraction of the baseline measurement per well. Cell numbers were quantified using a calibration  
166 curve displaying fluorescence as a function of cell number prepared with HeLa cells seeded in 96-  
167 well tissue culture plastic plates at densities of  $6.0 \times 10^4$ ,  $3.0 \times 10^4$ ,  $1.2 \times 10^4$ ,  $6.0 \times 10^3$ ,  $3.0 \times 10^3$  and  $0.6 \times 10^3$   
168 cells per well incubated at 37 °C, 5% CO<sub>2</sub> (Figure S3 – S5 in Supplementary Materials).

169 *Statistical analysis* was performed by one-way ANOVA followed by Bonferroni's post-test using  
170 Graphpad Prism 5.0 (USA). A  $p < 0.05$  was considered statistically significant. Results are presented  
171 as mean  $\pm$  standard deviation. Three independent biological experiments were prepared for each  
172 experiment.

### 173 3. Results and discussion

174 The well-defined lengths, ready functionalization of the terminal sites, and varied architectures  
175 made the multi-arm PEG architectures attractive scaffolds for the design and fabrication of a wide  
176 variety of hydrogels with different crosslinking chemistries [57]. Herein, the hydrogel precursor 4-  
177 armed PEG-aldehydes were prepared by nucleophilic substitution of commercially available 4-arm  
178 PEG-OH with 2-bromo-1,1-diethoxyethane, followed by acid hydrolysis of the acetal to yield the  
179 corresponding aliphatic 4-arm PEG-aldehydes.

180 4-arm PEG-aldehydes precursor was mixed with poly- $\epsilon$ -lysine at molar ratios 1:2 and 1:10,  
181 resulting in reversible crosslinking *via* imine formation in PBS (see Figure 1). Hydrogels were formed  
182 with concentrations of 4-armed PEG-aldehydes above 5% w/v at both molar ratios (see Figure S6 in  
183 Supplementary Materials). Similarly, 4-armed PEG-aldehydes were mixed with diamino-PEG to  
184 produce hydrogels at precursor concentrations above 8% w/v (see Figure S7 in Supplementary  
185 Materials). Generally, a faster gel formation was observed with higher 4-armed PEG-aldehydes  
186 precursor concentrations. The cell adhesive peptide motif RGD was synthesized in such a way that it  
187 would be incorporated into the hydrogel network as an additional crosslinker *via* dynamic imine  
188 bond formation with concentration levels between 0 and 20 mM. Gel formation was observed for all  
189 RGD constructs, but slower gelation was observed for gels with higher levels of RGD (see Figure 3  
190 A-C). For example, HG-PεK with a molar ratio of 1:2 with 0.2 mM RGD produced a gel after 2 hours,  
191 while with 20 mM gelation took over 6 hours at room temperature.



192

193

194

195

196

**Figure 1.** Hydrogels generated *via* dynamic imine crosslinking. The hydrogels were fabricated using either a 4-arm PEG each terminating in an aldehyde group and mixed with either poly- $\epsilon$ -lysine to give HG-P $\epsilon$ K or a linear diamine PEG to give HG-PEG. The peptide RGD was synthesized as a *bis*-amine and was added at differing concentrations to promote cell binding.

197

198

199

200

201

202

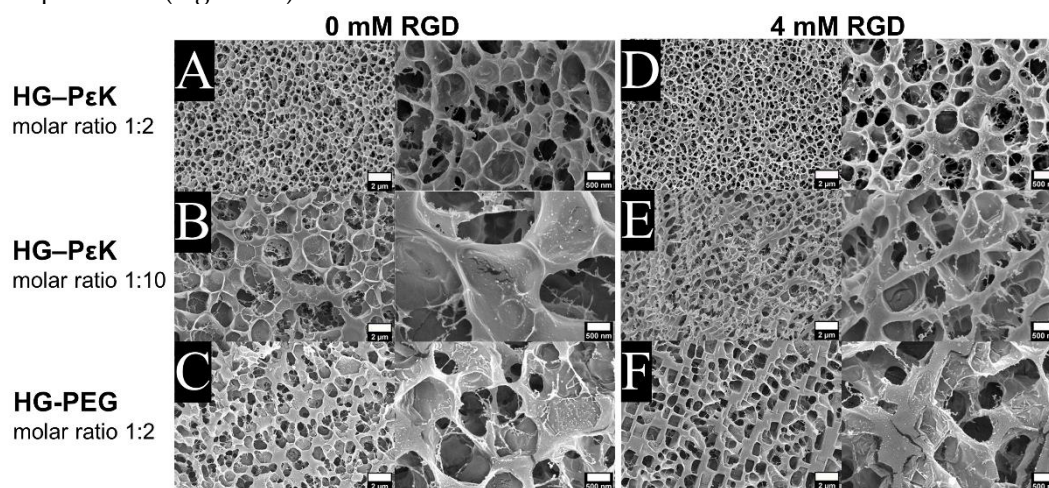
203

204

205

206

The internal structure of the hydrogel was imaged by cryo-SEM, with the microstructure of HG-P $\epsilon$ K and HG-PEG examined in the swollen state and compared to that of hydrogels containing the cell adhesive peptide RGD at 4 mM. Overall, all the cryo-dried hydrogels displayed a honeycomb-like 3D network structure with some notable differences in pore size. Smaller pores were observed for HG-P $\epsilon$ K in comparison to HG-PEG for constructs with a molar ratio 1:2 (Figure 2A and 2C). The addition of RGD had no visible effect on the hydrogel microstructure of either HG-P $\epsilon$ K or HG-PEG (Figure 2D and 2F). Increasing the P $\epsilon$ K molar ratio to 1:10 in HG-P $\epsilon$ K (Figure 2B), resulted in larger pore sizes than that of HG-P $\epsilon$ K with a molar ratio of 1:2. Here, the addition of RGD had a clear effect on the microstructure of HG-P $\epsilon$ K molar ratio 1:10, yielding a more compact microstructure with smaller pore sizes (Figure 2E).



207

208

209

210

211

212

**Figure 2.** Hydrogel internal structures imaged by Cryo-SEM. Left panel: Hydrogel morphology without the RGD peptide for (A) HG-P $\epsilon$ K molar ratio 1:2, (B) HG-P $\epsilon$ K molar ratio 1:10, and (C) HG-PEG molar ratio 1:2. Right panel: Hydrogel morphology with 4 mM RGD peptide for (D) HG-P $\epsilon$ K molar ratio 1:2, (E) HG-P $\epsilon$ K molar ratio 1:10, and (F) HG-PEG molar ratio 1:2. For each panel the scale bars in the left micrographs are 2  $\mu$ m and right micrographs are 500 nm.

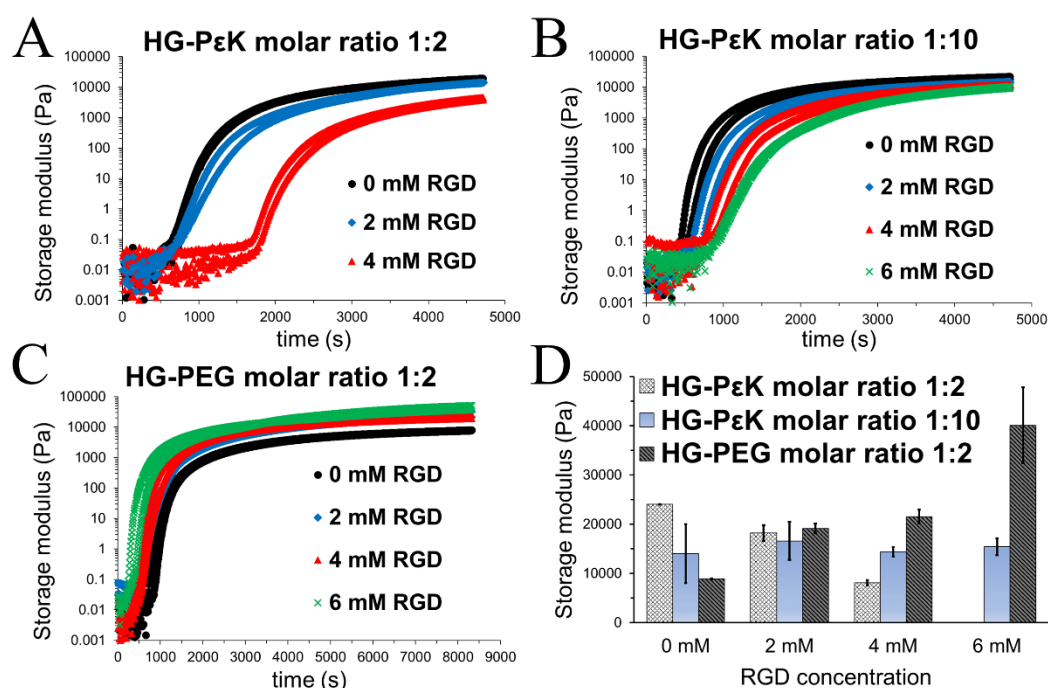
213

214

Oscillatory rheology time and frequency sweeps were performed to provide insight into the gelation time and stiffness of HG-P $\epsilon$ K and HG-PEG as a function of molar ratio and RGD

215 concentrations. HG-P $\epsilon$ K with a molar ratio of 1:2 in the absence of RGD had a delay in gelation rate  
 216 compared to HG-P $\epsilon$ K with a molar ratio of 1:10. This increase in gelation time presumably arises due  
 217 to fewer free poly- $\epsilon$ -lysine chains available during the reversible crosslinking. The sequential increase  
 218 of RGD concentration in HG-P $\epsilon$ K at both molar ratios led to weaker network structures with slower  
 219 gelation rates. This behavior was more evident at molar ratios of 1:2 probably due to the competition  
 220 of amine groups from the RGD and the poly- $\epsilon$ -lysine chains for reversible imine bond formation  
 221 (Figure 3A and 3B). On the other hand, the opposite behavior was observed for the HG-PEG gels with  
 222 rapid gelation time upon RGD addition (Figure 3C).

223 The storage moduli was obtained from frequency sweeps with a fixed strain of 1% (within the  
 224 linear viscoelastic region) as a function of RGD concentration (Figure S8-S10 in Supplementary  
 225 Materials). RGD negligibly contributed to the storage moduli in HG-P $\epsilon$ K with a molar ratio of 1:10  
 226 due to excess of poly- $\epsilon$ -lysine in the hydrogel formulation. In contrast, HG-P $\epsilon$ K and HG-PEG with a  
 227 molar ratio of 1:2 showed distinct and opposing storage moduli trends as a function of RGD  
 228 concentration. While the storage moduli decreased in HG-P $\epsilon$ K, the storage moduli in HG-PEG  
 229 increased with increases in RGD levels (Figure 3D). Overall the mechanical properties and cryo-SEM  
 230 analysis agreed with the higher storage moduli and the compact microstructure in HG-P $\epsilon$ K with a  
 231 molar ratio of 1:2, compared to the lower storage moduli and larger pore sizes found in HG-P $\epsilon$ K with  
 232 a molar ratio 1:10. On the other hand, the increase in the concentration of RGD led to significant  
 233 differences in HG-PEG storage moduli in both the absence and presence of RGD, despite similar  
 234 internal structure and pore size. Regardless of the opposite mechanical properties between HG-P $\epsilon$ K  
 235 and HG-PEG, the constructs had the same storage moduli when formulated at 2 mM RGD, indicative  
 236 of similar material stiffnesses at this peptide concentration.



237

238

239

240

241

242

243

244

245

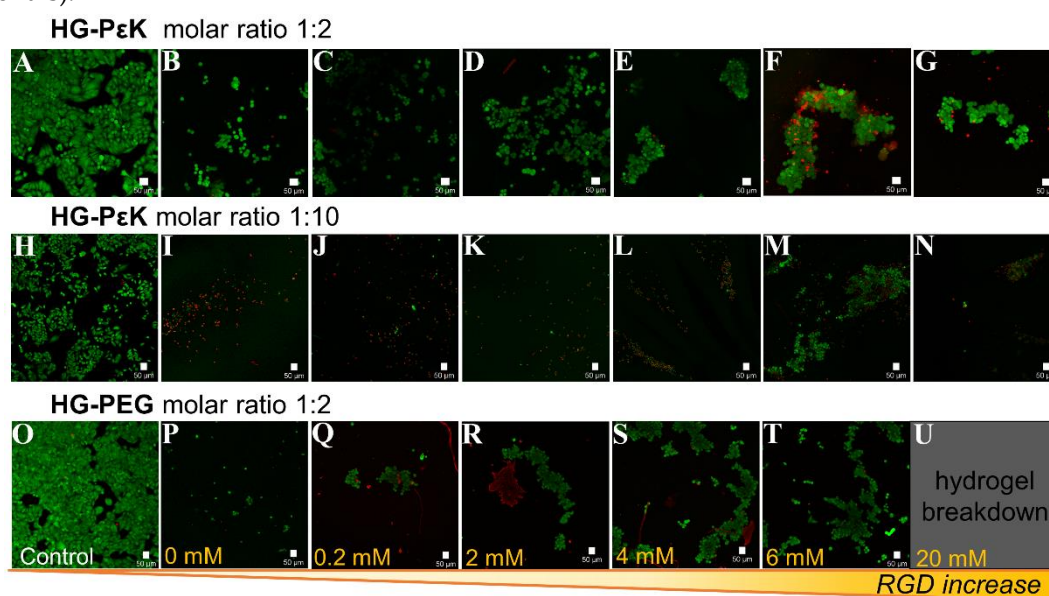
246

247

**Figure 3.** Hydrogel mechanical characterization by oscillatory rheology. Time sweep plots are displayed as two independent flow traces for each hydrogel construct as function of RGD concentration at 37 °C. (A) Time sweep for HG-P $\epsilon$ K molar ratio 1:2 with 0 mM RGD (black circle), 2 mM RGD (blue diamond) and 4 mM RGD (red triangle). (B) Time sweep for HG-P $\epsilon$ K molar ratio 1:10 with 0 mM RGD (black circle), 2 mM RGD (blue diamond), 4 mM RGD (red triangle) and 6 mM RGD (green cross). (C) Time sweep for HG-PEG molar ratio 1:2 with 0 mM RGD (black circle), 2 mM RGD (blue diamond), 4 mM RGD (red triangle) and 6 mM RGD (green cross). (D) Storage moduli as a function of RGD concentration at 37 °C. The storage moduli was obtained at 1 Hz from frequency sweeps in the linear viscoelastic region presented in Figure S8, Figure S9 and Figure S10 in Supplementary Materials. Data represents mean  $\pm$  standard deviation (n=2).

248 HG-PεK and HG-PEG constructs were interrogated for their ability to allow cellular adhesion  
 249 and proliferation as a function of RGD concentration using confocal microscopy (Figure 4). HeLa  
 250 cells, a common and widely laboratory available cell system, were seeded on the preformed RGD  
 251 hydrogel constructs and incubated for 48 hours at 37 °C and 5% CO<sub>2</sub>.

252 Imaging of cells on HG-PεK and HG-PEG at a 1:2 molar ratio in the absence of RGD showed  
 253 high cell viability with a higher number of cells observed in HG-PεK, indicative of the capability of  
 254 cells to interact with the hydrogel matrix. In contrast, higher numbers of dead cells were observed  
 255 for HG-PεK with a molar ratio of 1:10, with few cells surviving at higher concentrations of RGD. In  
 256 terms of cell morphology, ball-like cluster formations with high cell viability were observed in HG-  
 257 PεK with a molar ratio of 1:2 at all RGD concentrations, but with increasing numbers of dead cells at  
 258 higher RGD concentrations. Similarly, HG-PEG with a molar ratio of 1:2 gave ball-like cell cluster  
 259 formations with few dead cells at 0.2 mM RGD, while above this concentration string-like clusters  
 260 with high cell viability were observed along the strands of the hydrogel network structure, indicative  
 261 of the efficacy of RGD in promoting cell adhesion (Figure 4 and Figure S4 in Supplementary  
 262 Materials).



263

264 **Figure 4.** Live/dead cell viability staining of HeLa cells seeded on a dynamic hydrogel array with  
 265 varying levels of the peptide RGD. HeLa cells were seeded and incubated with complete DMEM for  
 266 48 hours at 37 °C and 5% CO<sub>2</sub> before imaging on (A, H and O) tissue culture plate, (B) HG-PεK molar  
 267 ratio 1:2 with 0 mM RGD, (C) HG-PεK molar ratio 1:2 with 0.2 mM RGD, (D) HG-PεK molar ratio 1:2  
 268 with 2 mM RGD, (E) HG-PεK molar ratio 1:2 with 4 mM RGD, (F) HG-PεK molar ratio 1:2 with 6 mM  
 269 RGD, (G) HG-PεK molar ratio 1:2 with 20 mM RGD, (I) HG-PεK molar ratio 1:10 with 0 mM RGD, (J)  
 270 HG-PεK molar ratio 1:10 with 0.2 mM RGD, (K) HG-PεK molar ratio 1:10 with 2 mM RGD, (L) HG-  
 271 PεK molar ratio 1:10 with 4 mM RGD, (M) HG-PεK molar ratio 1:10 with 6 mM RGD, (N) HG-PεK  
 272 molar ratio 1:10 with 20 mM RGD, (P) HG-PEG molar ratio 1:2 with 0 mM RGD, (Q) HG-PEG molar  
 273 ratio 1:2 with 0.2 mM RGD, (R) HG-PEG molar ratio 1:2 with 2 mM RGD, (S) HG-PEG molar ratio 1:2  
 274 with 4 mM RGD, (T) HG-PEG molar ratio 1:2 with 6 mM RGD, and (U) HG-PEG molar ratio 1:2 with  
 275 20 mM RGD. Live cells are in green and dead cells are in red. Scale bars are 50 μm.

276 Additionally, HeLa cell viability/proliferation capability on the hydrogels was assessed using an  
 277 AlamarBlue assay (Figure 5). 2.0×10<sup>4</sup> HeLa cells per well were seeded on tissue culture plastic (TCP),  
 278 HG-PεK, and HG-PEG at a molar ratio of 1:2 with differing concentrations of RGD.

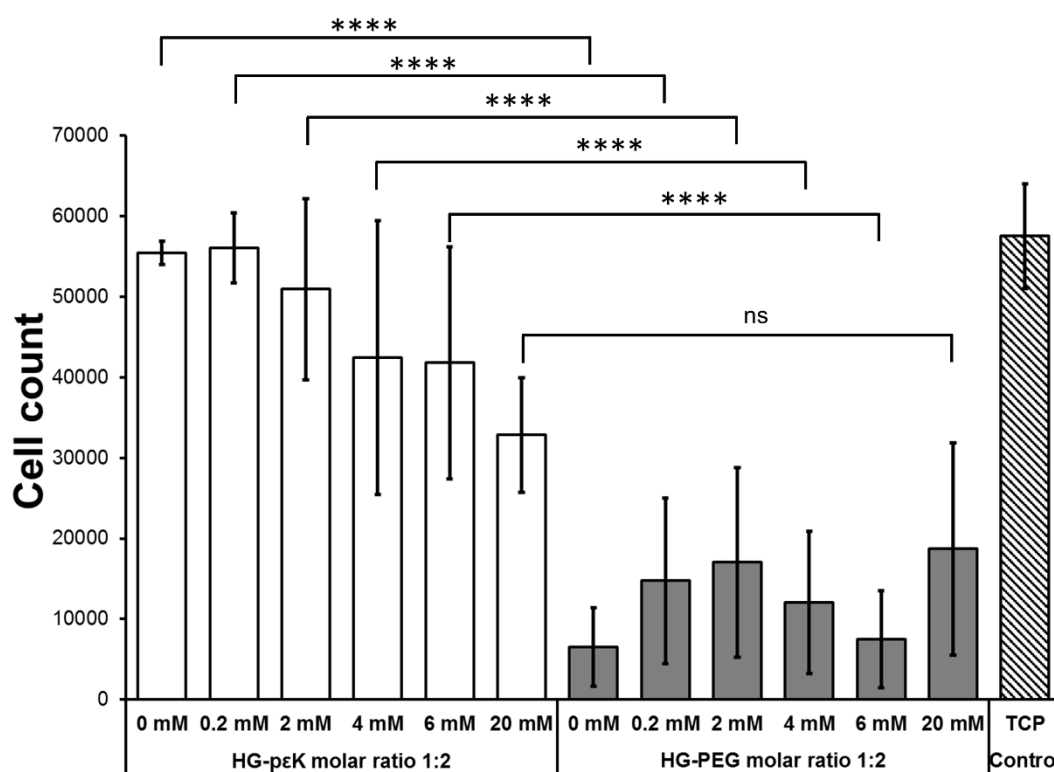
279 On TCP after 48 hours incubation time a three-fold cell increase was observed. A similar cell  
 280 increase was observed for HG-PεK with molar ratio 1:2 in the absence of RGD (no significant  
 281 difference,  $p > 0.05$ ) while HG-PEG with a molar ratio of 1:2 (without RGD) showed the opposite  
 282 behavior with a three-fold decrease in cells (significantly different,  $p \leq 0.0001$ ) compared to TCP and  
 283 HG-PεK in the absence of RGD. RGD levels in HG-PεK and HG-PEG resulted in significantly



284 different increases in cell number, with HG-PεK having a three-fold increase in cell number ( $p \leq$   
 285 0.0001) at 0.2 and 2 mM RGD and a significantly different two-fold cell increase ( $p \leq 0.0001$ ) at 4 and  
 286 6 mM RGD after 48 hours. No significant difference was observed between HG-PεK and HG-PEG at  
 287 20 mM RGD. These results were indicative of good cell viability and proliferation on HG-PεK within  
 288 the RGD concentration range analyzed from 0 to 6 mM. On the other hand, no cell proliferation was  
 289 detected on HG-PEG in line with cell viabilities reported in conventional chemically crosslinked PEG  
 290 hydrogels containing RGD [58].

291 Overall, hydrogels containing poly-ε-lysine were successfully formed using dynamic imine  
 292 crosslinking. High quantities of poly-ε-lysine in the hydrogel formulation improved the storage  
 293 moduli of gels and gelation time compared to low poly-ε-lysine levels (molar ratio 1:2 relative to  
 294 crosslinker). In contrast, low levels of poly-ε-lysine improved cell viability but a too high ratio of  
 295 poly-ε-lysine was detrimental to cell viability. This cytotoxicity at high levels of poly-ε-lysine (molar  
 296 ratio 1:10 relative to crosslinker) arises due to excesses of free amines in the hydrogel scaffold, in  
 297 agreement with reported cytotoxicity for polymeric biomaterials with high free amine concentrations  
 298 [51].

299 Oscillatory rheology and cryo-SEM characterization showed that HG-PεK with a molar ratio of  
 300 1:2 formed a stiffer construct compared to HG-PEG; a non-fouling hydrogel broadly used for 3D cell  
 301 culture. Interestingly, the incorporation of high levels of the *bis*-amine RGD peptide resulted in softer  
 302 HG-PεK constructs, while the expected crosslinking effect was detected in HG-PEG with increasing  
 303 levels of RGD leading to stiffer constructs. Despite this unexpected difference in mechanical  
 304 properties with the incorporation of RGD in the hydrogel formulation, HG-PεK constructs displayed  
 305 good cytocompatibility with higher metabolic activity/viability detected in HG-PεK with 0 and 0.2  
 306 mM of RGD leading to three-fold increase in cell number after 48 hours cell culture. Cell adhesion  
 307 and metabolic activity have been reported in chemically static poly-ε-lysine hydrogels with enhanced  
 308 stiffness (Young modulus of 0.11 MPa) [52]. Here, these investigations demonstrated that the  
 309 dynamic crosslinked HG-PεK with molar ratio of 1:2 (storage moduli of 0.02 MPa) formulated with  
 310 low RGD concentrations provided enough stability and structural support, like chemically static  
 311 poly-ε-lysine hydrogels, to afford cellular adhesion and proliferation.  
 312



314 **Figure 5.** HeLa cell proliferation capability on HG-PεK and HG-PEG with molar ratios of 1:2 and  
315 varying levels of RGD. AlamarBlue metabolic activity assay after 48 hours cell incubation (see Figure  
316 S3, S4 and S5 in Supplementary Materials). TCP control experiment corresponds to cells seeded on  
317 tissue culture plate. Cell count on hydrogels confirmed live/dead cell viability experiments for the  
318 HG-PεK and HG-PEG gels. Cell number analysis indicated higher cell proliferation rates on HG-PεK  
319 after 48 hours compared to cells cultured on the HG-PEG constructs. One-way ANOVA with  
320 Bonferroni post-test (ns = no significant \*  $p \leq 0.05$ , \*\*  $p \leq 0.01$ , \*\*\*  $p \leq 0.001$ , and \*\*\*\*  $p \leq 0.0001$ ). Data  
321 represents mean  $\pm$  standard deviation (n=3).

#### 322 4. Conclusion

323 Using reversible Schiff-base bond formation, hydrogels containing poly-ε-lysine and PEG were  
324 prepared to evaluate their feasibility for cell culture. The use of poly-ε-lysine proved advantageous  
325 because of its simple formulation yielding gels *via* reversible imine formation using low quantities of  
326 material. This is in comparison to other natural polymer precursors that can require further  
327 functionalization to produce dynamic crosslinking. HG-PεK with low molar ratios of poly-ε-lysine  
328 resulted in suitable candidates for cell culture that displayed good cell adhesion and  
329 cytocompatibility. The cell binding RGD peptide was incorporated into the hydrogel network to  
330 enhance cell adhesion and biomechanical material properties. The metabolic activity of cells on the  
331 biomaterial was measured with the AlamarBlue assay, indicating higher metabolic activity in HG-  
332 PεK with low levels of RGD than in HG-PEG. In this study dynamic poly-ε-lysine hydrogels were  
333 generated with RGD but this approach is highly tunable, for example differing cell adhesive ligands  
334 such as laminin could be readily added for cell culture of other mammalian cells.

335 **Supplementary Materials:** The following are available online at [www.mdpi.com/xxx/s1](http://www.mdpi.com/xxx/s1), Figure S1: <sup>1</sup>H NMR  
336 spectrum 4-arm PEG-aldehydes, Figure S2: FT-IR spectra for 4-arm PEG-OH and 4-arm PEG-aldehydes, Table  
337 S1: Formulation of HG-PεK (molar ratio 1:2) with varying levels of the peptide RGD, Table S2: Formulation of  
338 HG-PεK (molar ratio 1:10) with varying levels of the peptide RGD, Table S3: Formulation of HG-PEG (molar  
339 ratio 1:2) with varying levels of the peptide RGD, Figure S3: Brightfield microscopy of HeLa cell seeded on tissue  
340 culture plastic for AlamarBlue assay, Figure S4: Brightfield microscopy of cells seeded at density of 20,000 on  
341 dynamic hydrogels and incubated in complete DMEM at 37 °C and 5% CO<sub>2</sub> for AlamarBlue assay, Figure S5:  
342 Calibration curve fluorescence *vs* cell number, Figure S6: Images of HG-PεK (molar ratio 1:2) formulated at  
343 differing concentrations of 4-arm PEG-aldehydes, Figure S7: Images of HG-PEG (molar ratio 1:2) formulated at  
344 differing concentrations of 4-arm PEG-aldehydes, Figure S8: Frequency sweep plots of HG-PεK (molar ratio 1:2)  
345 with 0, 2 and 4 mM RGD at constant strain of 1% at 37 °C, Figure S9: Frequency sweep plots of HG-PεK (molar  
346 ratio 1:10) with 0, 2, 4 and 6 mM RGD at constant strain of 1% at 37 °C, Figure S10: Frequency sweep plots of  
347 HG-PEG (molar ratio 1:2) with 0, 2, 4 and 6 mM RGD at constant strain of 1% at 37 °C.

348 **Author Contributions:** Conceptualization, N.L.M. and M.B.; validation, N.L.M., M.O., S.S., and A.F.S.; formal  
349 analysis, N.L.M and M.O.; writing—original draft preparation, N.L.M.; writing—review and editing, M.O., S.S.,  
350 A.F.S., and M.B.; funding acquisition, M.B. All authors have read and agreed to the published version of the  
351 manuscript.

352 **Funding:** This research was funded by an ERC Advanced Grant, grant number ERC-2013-ADG 340469  
353 ADREEM.

354 **Acknowledgments:** Dr. Thomas Glen is acknowledged for his technical support with Cryo-SEM imaging. Cryo-  
355 SEM was conducted at the Cryo FIB-SEM facilities in the Institute for Condensed Matter and Complex Systems  
356 (ICMCS), Edinburgh, UK. Oscillatory rheology was conducted at the Edinburgh Complex Fluids Partnership  
357 facilities in the ICMCS, Edinburgh, UK. Confocal imaging was conducted at the CALM facilities in the QMRI,  
358 Edinburgh, UK.

359 **Conflicts of Interest:** The authors declare no conflict of interest.

#### 360 References

- 361 1. Wang, H.; Heilshorn, S.C., Adaptable hydrogel networks with reversible linkages for tissue  
362 engineering. *Advanced materials* **2015**, *27*, 3717-3736.

- 363 2. Zhu, J.; Marchant, R.E., Design properties of hydrogel tissue-engineering scaffolds. *Expert review of*  
364 *medical devices* **2011**, *8*, 607-626.
- 365 3. Ghobril, C.; Grinstaff, M.W., The chemistry and engineering of polymeric hydrogel adhesives for  
366 wound closure: A tutorial. *Chemical Society Reviews* **2015**, *44*, 1820-1835.
- 367 4. Giano, M.C.; Ibrahim, Z.; Medina, S.H.; Sarhane, K.A.; Christensen, J.M.; Yamada, Y.; Brandacher, G.;  
368 Schneider, J.P., Injectable bioadhesive hydrogels with innate antibacterial properties. *Nature*  
369 *communications* **2014**, *5*, 4095.
- 370 5. Xinming, L.; Yingde, C.; Lloyd, A.W.; Mikhalovsky, S.V.; Sandeman, S.R.; Howel, C.A.; Liewen, L.,  
371 Polymeric hydrogels for novel contact lens-based ophthalmic drug delivery systems: A review. *Contact*  
372 *lens & anterior eye : the journal of the British Contact Lens Association* **2008**, *31*, 57-64.
- 373 6. Gallagher, A.G.; Alorabi, J.A.; Wellings, D.A.; Lace, R.; Horsburgh, M.J.; Williams, R.L., A novel peptide  
374 hydrogel for an antimicrobial bandage contact lens. *Advanced healthcare materials* **2016**, *5*, 2013-2018.
- 375 7. Li, J.; Mooney, D.J., Designing hydrogels for controlled drug delivery. *Nature Reviews Materials* **2016**, *1*,  
376 16071.
- 377 8. Buenger, D.; Topuz, F.; Groll, J., Hydrogels in sensing applications. *Progress in Polymer Science* **2012**, *37*,  
378 1678-1719.
- 379 9. Zhang, Y.S.; Khademhosseini, A., Advances in engineering hydrogels. *Science* **2017**, 356.
- 380 10. Tan, Y.; Huang, H.; Ayers, D.C.; Song, J., Modulating viscoelasticity, stiffness, and degradation of  
381 synthetic cellular niches via stoichiometric tuning of covalent versus dynamic noncovalent cross-  
382 linking. *ACS central science* **2018**, *4*, 971-981.
- 383 11. Chu, S.; Sridhar, S.L.; Akalp, U.; Skaalure, S.C.; Vernerey, F.J.; Bryant, S.J., (\*) understanding the  
384 spatiotemporal degradation behavior of aggrecanase-sensitive poly(ethylene glycol) hydrogels for use  
385 in cartilage tissue engineering. *Tissue engineering. Part A* **2017**, *23*, 795-810.
- 386 12. Bryant, S.J.; Anseth, K.S., Controlling the spatial distribution of ecm components in degradable peg  
387 hydrogels for tissue engineering cartilage. *Journal of biomedical materials research. Part A* **2003**, *64*, 70-79.
- 388 13. Lutolf, M.P.; Lauer-Fields, J.L.; Schmoekel, H.G.; Metters, A.T.; Weber, F.E.; Fields, G.B.; Hubbell, J.A.,  
389 Synthetic matrix metalloproteinase-sensitive hydrogels for the conduction of tissue regeneration:  
390 Engineering cell-invasion characteristics. *Proceedings of the National Academy of Sciences* **2003**, *100*, 5413-  
391 5418.
- 392 14. Patterson, J.; Hubbell, J.A., Enhanced proteolytic degradation of molecularly engineered peg hydrogels  
393 in response to mmp-1 and mmp-2. *Biomaterials* **2010**, *31*, 7836-7845.
- 394 15. Wojtecki, R.J.; Meador, M.A.; Rowan, S.J., Using the dynamic bond to access macroscopically  
395 responsive structurally dynamic polymers. *Nature Materials* **2011**, *10*, 14-27.
- 396 16. Foster, E.M.; Lensmeyer, E.E.; Zhang, B.; Chakma, P.; Flum, J.A.; Via, J.J.; Sparks, J.L.; Konkolewicz, D.,  
397 Effect of polymer network architecture, enhancing soft materials using orthogonal dynamic bonds in  
398 an interpenetrating network. *ACS Macro Letters* **2017**, *6*, 495-499.
- 399 17. Martínez-Sanz, E.; Ossipov, D.A.; Hilborn, J.; Larsson, S.; Jonsson, K.B.; Varghese, O.P., Bone reservoir:  
400 Injectable hyaluronic acid hydrogel for minimal invasive bone augmentation. *Journal of Controlled*  
401 *Release* **2011**, *152*, 232-240.
- 402 18. Han, X.; Meng, X.; Wu, Z.; Wu, Z.; Qi, X., Dynamic imine bond cross-linked self-healing thermosensitive  
403 hydrogels for sustained anticancer therapy via intratumoral injection. *Materials Science and Engineering:*  
404 *C* **2018**, *93*, 1064-1072.
- 405 19. Mukherjee, S.; Hill, M.R.; Sumerlin, B.S., Self-healing hydrogels containing reversible oxime crosslinks.  
406 *Soft Matter* **2015**, *11*, 6152-6161.
- 407 20. Yu, H.; Wang, Y.; Yang, H.; Peng, K.; Zhang, X., Injectable self-healing hydrogels formed via  
408 thiol/disulfide exchange of thiol functionalized f127 and dithiolane modified peg. *Journal of Materials*  
409 *Chemistry B* **2017**, *5*, 4121-4127.
- 410 21. Rosales, A.M.; Anseth, K.S., The design of reversible hydrogels to capture extracellular matrix  
411 dynamics. *Nature reviews. Materials* **2016**, *1*.
- 412 22. Han, X.; Meng, X.; Wu, Z.; Wu, Z.; Qi, X., Dynamic imine bond cross-linked self-healing thermosensitive  
413 hydrogels for sustained anticancer therapy via intratumoral injection. *Materials science & engineering. C,*  
414 *Materials for biological applications* **2018**, *93*, 1064-1072.
- 415 23. Huang, W.; Wang, Y.; Chen, Y.; Zhao, Y.; Zhang, Q.; Zheng, X.; Chen, L.; Zhang, L., Strong and rapidly  
416 self-healing hydrogels: Potential hemostatic materials. *Advanced healthcare materials* **2016**, *5*, 2813-2822.
- 417 24. Li, J.; Viveros, J.A.; Wrue, M.H.; Anthamatten, M., Shape-memory effects in polymer networks  
418 containing reversibly associating side-groups. *Advanced materials* **2007**, *19*, 2851-2855.
- 419 25. Chujo, Y.; Sada, K.; Naka, A.; Nomura, R.; Saegusa, T., Synthesis and redox gelation of disulfide-  
420 modified polyoxazoline. *Macromolecules* **1993**, *26*, 883-887.

- 421 26. Kinami, M.; Crenshaw, B.R.; Weder, C., Polyesters with built-in threshold temperature and  
422 deformation sensors. *Chemistry of Materials* **2006**, *18*, 946-955.
- 423 27. Otsuka, H.; Nagano, S.; Kobashi, Y.; Maeda, T.; Takahara, A., A dynamic covalent polymer driven by  
424 disulfide metathesis under photoirradiation. *Chemical Communications* **2010**, *46*, 1150-1152.
- 425 28. Geckil, H.; Xu, F.; Zhang, X.; Moon, S.; Demirci, U., Engineering hydrogels as extracellular matrix  
426 mimics. *Nanomedicine* **2010**, *5*, 469-484.
- 427 29. Tibbitt, M.W.; Anseth, K.S., Hydrogels as extracellular matrix mimics for 3d cell culture. *Biotechnology  
428 and Bioengineering* **2009**, *103*, 655-663.
- 429 30. Zhang, Y.; Tao, L.; Li, S.; Wei, Y., Synthesis of multiresponsive and dynamic chitosan-based hydrogels  
430 for controlled release of bioactive molecules. *Biomacromolecules* **2011**, *12*, 2894-2901.
- 431 31. Karimi, A.R.; Khodadadi, A., Mechanically robust 3d nanostructure chitosan-based hydrogels with  
432 autonomic self-healing properties. *ACS Applied Materials & Interfaces* **2016**, *8*, 27254-27263.
- 433 32. Pettignano, A.; Häring, M.; Bernardi, L.; Tanchoux, N.; Quignard, F.; Díaz Díaz, D., Self-healing  
434 alginate-gelatin biohydrogels based on dynamic covalent chemistry: Elucidation of key parameters.  
435 *Materials Chemistry Frontiers* **2017**, *1*, 73-79.
- 436 33. Gillette, B.M.; Jensen, J.A.; Wang, M.; Tchao, J.; Sia, S.K., Dynamic hydrogels: Switching of 3d  
437 microenvironments using two-component naturally derived extracellular matrices. *Advanced materials*  
438 **2010**, *22*, 686-691.
- 439 34. Vahedi, M.; Barzin, J.; Shokrolahi, F.; Shokrollahi, P., Self-healing, injectable gelatin hydrogels cross-  
440 linked by dynamic schiff base linkages support cell adhesion and sustained release of antibacterial  
441 drugs. *Macromolecular Materials and Engineering* **2018**, *303*, 1800200.
- 442 35. Choh, S.Y.; Cross, D.; Wang, C., Facile synthesis and characterization of disulfide-cross-linked  
443 hyaluronic acid hydrogels for protein delivery and cell encapsulation. *Biomacromolecules* **2011**, *12*, 1126-  
444 1136.
- 445 36. Alakpa, E.V.; Jayawarna, V.; Burgess, K.E.V.; West, C.C.; Péault, B.; Ulijn, R.V.; Dalby, M.J., Improving  
446 cartilage phenotype from differentiated pericytes in tunable peptide hydrogels. *Scientific Reports* **2017**,  
447 *7*, 6895.
- 448 37. Silva, A.K.A.; Richard, C.; Bessodes, M.; Scherman, D.; Merten, O.-W., Growth factor delivery  
449 approaches in hydrogels. *Biomacromolecules* **2009**, *10*, 9-18.
- 450 38. Fears, C.Y.; Woods, A., The role of syndecans in disease and wound healing. *Matrix Biology* **2006**, *25*,  
451 443-456.
- 452 39. Ruoslahti, E.; Pierschbacher, M., New perspectives in cell adhesion: Rgd and integrins. *Science* **1987**,  
453 *238*, 491-497.
- 454 40. Wang, F.; Li, Y.; Shen, Y.; Wang, A.; Wang, S.; Xie, T., The functions and applications of rgd in tumor  
455 therapy and tissue engineering. *International journal of molecular sciences* **2013**, *14*, 13447-13462.
- 456 41. Hirano, Y.; Okuno, M.; Hayashi, T.; Goto, K.; Nakajima, A., Cell-attachment activities of surface  
457 immobilized oligopeptides rgd, rgds, rgdv, rgdt, and yigsr toward five cell lines. *Journal of Biomaterials  
458 Science, Polymer Edition* **1993**, *4*, 235-243.
- 459 42. Cheng, S.; Craig, W.S.; Mullen, D.; Tschopp, J.F.; Dixon, D.; Pierschbacher, M.D., Design and synthesis  
460 of novel cyclic rgd-containing peptides as highly potent and selective integrin .Alpha.lib.Beta.3  
461 antagonists. *Journal of Medicinal Chemistry* **1994**, *37*, 1-8.
- 462 43. Hersel, U.; Dahmen, C.; Kessler, H., Rgd modified polymers: Biomaterials for stimulated cell adhesion  
463 and beyond. *Biomaterials* **2003**, *24*, 4385-4415.
- 464 44. Antonova, L.V.; Silnikov, V.N.; Sevostyanova, V.V.; Yuzhalin, A.E.; Koroleva, L.S.; Velikanova, E.A.;  
465 Mironov, A.V.; Godovikova, T.S.; Kutikhin, A.G.; Glushkova, T.V., *et al.*, Biocompatibility of small-  
466 diameter vascular grafts in different modes of rgd modification. *Polymers* **2019**, *11*.
- 467 45. Maynard, H.D.; Okada, S.Y.; Grubbs, R.H., Inhibition of cell adhesion to fibronectin by oligopeptide-  
468 substituted polynorbornenes. *Journal of the American Chemical Society* **2001**, *123*, 1275-1279.
- 469 46. Comisar, W.A.; Kazmers, N.H.; Mooney, D.J.; Linderman, J.J., Engineering rgd nanopatterned  
470 hydrogels to control preosteoblast behavior: A combined computational and experimental approach.  
471 *Biomaterials* **2007**, *28*, 4409-4417.
- 472 47. Boturny, D.; Coll, J.-L.; Garanger, E.; Favrot, M.-C.; Dumy, P., Template assembled cyclopeptides as  
473 multimeric system for integrin targeting and endocytosis. *Journal of the American Chemical Society* **2004**,  
474 *126*, 5730-5739.
- 475 48. Hyldgaard, M.; Mygind, T.; Vad, B.S.; Stenvang, M.; Otzen, D.E.; Meyer, R.L., The antimicrobial  
476 mechanism of action of epsilon-poly-l-lysine. *Appl Environ Microbiol* **2014**, *80*, 7758-7770.

- 477 49. Hiraki, J.; Ichikawa, T.; Ninomiya, S.-i.; Seki, H.; Uohama, K.; Seki, H.; Kimura, S.; Yanagimoto, Y.;  
478 Barnett, J.W., Use of adme studies to confirm the safety of  $\epsilon$ -polylysine as a preservative in food.  
479 *Regulatory Toxicology and Pharmacology* **2003**, *37*, 328-340.
- 480 50. Yoshida, T.; Nagasawa, T., E-poly-l-lysine: Microbial production, biodegradation and application  
481 potential. *Applied Microbiology and Biotechnology* **2003**, *62*, 21-26.
- 482 51. Wang, Y.-X.; Robertson, J.L.; Spillman, W.B.; Claus, R.O., Effects of the chemical structure and the  
483 surface properties of polymeric biomaterials on their biocompatibility. *Pharmaceutical Research* **2004**, *21*,  
484 1362-1373.
- 485 52. Kennedy, S.; Lace, R.; Carserides, C.; Gallagher, A.G.; Wellings, D.A.; Williams, R.L.; Levis, H.J., Poly-  
486  $\epsilon$ -lysine based hydrogels as synthetic substrates for the expansion of corneal endothelial cells for  
487 transplantation. *Journal of Materials Science: Materials in Medicine* **2019**, *30*, 102.
- 488 53. Wang, R.; Li, J.; Chen, W.; Xu, T.; Yun, S.; Xu, Z.; Xu, Z.; Sato, T.; Chi, B.; Xu, H., A biomimetic mussel-  
489 inspired  $\epsilon$ -poly-l-lysine hydrogel with robust tissue-anchor and anti-infection capacity. *Advanced*  
490 *Functional Materials* **2017**, *27*, 1604894.
- 491 54. Nicolas, J.; Magli, S.; Rabbachin, L.; Sampaolesi, S.; Nicotra, F.; Russo, L., 3d extracellular matrix mimics:  
492 Fundamental concepts and role of materials chemistry to influence stem cell fate. *Biomacromolecules*  
493 **2020**, *21*, 1968-1994.
- 494 55. Wacker, B.K.; Alford, S.K.; Scott, E.A.; Das Thakur, M.; Longmore, G.D.; Elbert, D.L., Endothelial cell  
495 migration on rgd-peptide-containing peg hydrogels in the presence of sphingosine 1-phosphate.  
496 *Biophysical journal* **2008**, *94*, 273-285.
- 497 56. Boehnke, N.; Cam, C.; Bat, E.; Segura, T.; Maynard, H.D., Imine hydrogels with tunable degradability  
498 for tissue engineering. *Biomacromolecules* **2015**, *16*, 2101-2108.
- 499 57. Parada, G.A.; Zhao, X., Ideal reversible polymer networks. *Soft Matter* **2018**, *14*, 5186-5196.
- 500 58. Phelps, E.A.; Enemchukwu, N.O.; Fiore, V.F.; Sy, J.C.; Murthy, N.; Sulchek, T.A.; Barker, T.H.; García,  
501 A.J., Maleimide cross-linked bioactive peg hydrogel exhibits improved reaction kinetics and cross-  
502 linking for cell encapsulation and in situ delivery. *Advanced materials* **2012**, *24*, 64-70.
- 503

